ACS APPLIED MATERIALS & INTERFACES

Research Article

www.acsami.org

A Modified Sol–Gel Technique for Pore Size Control in Porous Aluminum Oxide Nanowire Templates

Daniel N. Kelly,*,† Ryo H. Wakabayashi,‡ and Angelica M. Stacy

Department of Chemistry, University of California at Berkeley, Berkeley, California 94720, United States

ABSTRACT: A modified sol–gel technique was developed to continuously vary the pore diameters in porous alumina templates for the purpose of growing nanowires. To coat the pore walls, the porous alumina film is initially soaked in a methanol/water solution to fill the pores with the desired concentration of water. The porous alumina film is then exposed to a solution of 3-aminopropyltriethoxysilane (APTES) in toluene, creating a surface layer of APTES. The concentration of water in the pores correlates with the thickness of the APTES polymer coating that is obtained. This approach exerts greater control over the extent of silane polymerization than traditional sol–gel reactions by limiting the amount of water present for reaction. Factors such as the APTES concentration, exposure time, and organic cosolvent choice did not influence the coating thickness. However, the density and thickness of the APTES coating can be manipulated by varying the pH of the methanol/water solution as well as post-treatment annealing. Further modification of the pore size was achieved by subsequent reaction of the APTES coating with poly(methyl methacrylate) (PMMA). The PMMA couples to amine groups on the APTES polymer surface by an aminolysis reaction. Bismuth telluride nanowires were electrodeposited in the polymer-coated porous alumina templates using previously established methods. Nanowire diameters were smaller when the nanowires were prepared in modified templates as anticipated.

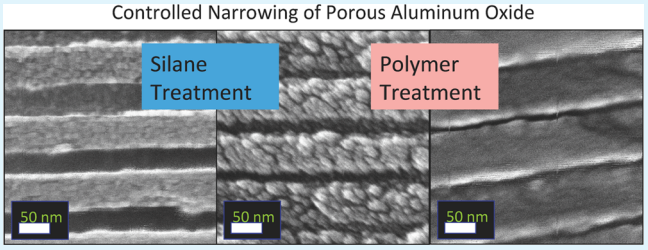

KEYWORDS: *porous aluminum oxide, sol–gel chemistry, nanowire templating*

INTRODUCTION

Although porous aluminum oxide (alumina) was originally developed in the 1940s and 1950s,[1,2] efforts to understand and modify this material for applications that can take advantage of the nanoporous structure have continued.[3−5] In particular, the monodisperse, nanoscale pores can be used as supports for catalysts,[6−8] for chromatographic and filtration applications,[9] as optical traps,[10] and as a template for nanomaterials.[11−15] One limitation of porous alumina is the lack of a continuous range of available pore diameters; in general, well-ordered pores have specific diameters related to the anodization potential and solution used for preparation (e.g., oxalic acid vs sulfuric acid). Although porous alumina can be prepared with pores ranging in diameter from <20 to >200 nm,[3,16−18] the pore diameters in well-ordered materials are not continuously variable within this range. This impacts the size specificity of filters and the sizes of nanomaterials prepared in porous alumina templates. In this paper, a study of coating the pores with varying thicknesses of 3-aminopropyltriethoxysilane (APTES) to vary the pore diameters in porous alumina is reported.

Use of porous alumina in nanowire synthesis is well-documented,[12−15,19−22] specifically the electrodeposition of nanowire arrays in metal-backed porous alumina templates. The template acts as a mask on the metal electrode surface, causing material deposition to conform to the pore shape and creating a nanostructured material. A templated array of nanowires has device implementation benefits versus single wires because of the forced alignment of all the nanowires and the structural support provided by the alumina template. A porous alumina film can be grown with an area in excess of 100 cm^2 and a thickness in excess of 100 μm with billions of nanopores.[20] These dimensions are suitable for incorporation of a nanowire-filled template into macroscale devices,[23] and this is a potentially useful way of utilizing the emergent properties found in nanoscale-confined systems. Tuning of pore diameters utilizing polymer coatings on the surfaces of the pores has the potential to allow for optimization of the nanowire properties through variations in the wire diameters.

Thermoelectric applications of nanowire arrays provide one example of the potential usefulness of polymer modification of porous alumina templates. While porous alumina is a template of choice because of the dense array of well-ordered pores with lengths of >100 μm, the material properties of porous alumina have some drawbacks. The minimal pore size is too large in many materials to reach the quantum confinement regime of a <20 nm wire diameter. It is at these small diameters that large changes in properties are predicted.[24−28] Additionally, the thermal conductivity of porous alumina is 40 W m^{-1} K^{-1}, a relatively high value for thermal applications. Coating the walls of porous alumina with a more thermally insulating polymer will decrease the pore size while helping to insulate nanowires from the alumina. Thus, polymer-coated porous alumina would

Received: August 25, 2014
Accepted: November 4, 2014
Published: November 12, 2014

offer the ability to study the effects on thermoelectric properties caused by systematic changes in wire diameter, as well as the ability to reach the sub-20 nm diameter wires in templates that are more thermally isolated than uncoated templates. In this study, the growth of thermoelectric nanowires with pore diameters of ∼20 nm in polymer-coated alumna templates is examined.

There are established methods for decreasing the pore diameter in porous alumina by filling in pores with metal oxide coatings. Sol−gel methods were originally applied to porous alumina by Martin et al.[12] A metal oxide precursor, such as alkoxysilane, is made into a sol, and the alumina is dipped in the sol for an appropriate length of time. The sol reacts with hydroxyl sites on the alumina surface and eventually builds into a thick surface layer of metal oxide. Fine-tuning of the coating thickness, and thus pore diameter, is difficult under these conditions because of the nature and timing of the dip with respect to mass transport and reaction kinetics. Another method for coating porous alumina surfaces is atomic layer deposition (ALD), developed by Stair et al.,[29,30] in which layers of atoms can be added sequentially to the pore walls. This provides incredibly precise control of pore diameter but comes at a cost of throughput and scalability because of the instrumentation required. Recent work has expanded the use of wet chemical etching to systematically widen pores in porous alumina.[31−33] These methods use phosphoric acid to slowly etch away alumina from the pore walls but have drawbacks with thick templates (>50 μm) because of mass-transfer issues. Long-range diffusion down the pores is slow, and the etch can introduce a conical shape to the pores, with wider diameters at the opening of the alumina.

In this work, we describe a method for adjusting the pore diameter in porous alumina by depositing an APTES polymer coating (shown in Figure 1, top), with design aims toward

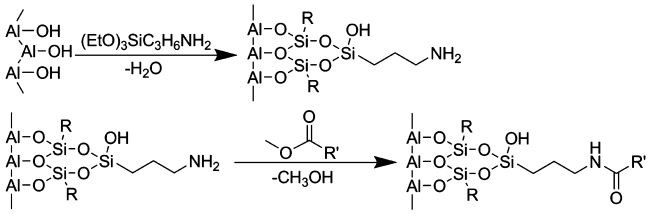

Figure 1. Reactions of APTES and PMMA with the alumina surface. Step 1 illustrates the attachment of the APTES layer (R = propylamine), while step 2 illustrates the aminolysis between PMMA and the APTES surface amines (R′ = polymer backbone).

enhancing thermoelectric nanowire arrays in thick porous alumina films. The alumina template is first soaked in a solution with a varying water/methanol composition to introduce a specific amount of water into the pores. After the template has been sufficiently filled, it is submerged into a toluene solution containing 3-aminopropyltriethoxysilane (APTES). This results in the attachment of APTES molecules to the pore walls through condensation with hydroxyl groups on the alumna; this is typically termed silanization. The water inside the pores is used to cross-link individual APTES molecules with one another, allowing more than monolayer coverage of the alumina surface. Via the control of the water composition of the solution in which the template is pretreated, it is possible to control the thickness of the APTES coating in the alumina pore by limiting the amount of water available for cross-linking APTES monomers. In this treatment, the water acts as the limiting reagent in APTES film growth. The use of APTES, rather than an inorganic silane precursor, allows us to further modify the pore surface in the porous alumina. Through an aminolysis reaction, we can couple the ester groups of poly(methyl methacrylate) (PMMA) with the amine group of APTES (Figure 1, bottom). This will further decrease the pore diameter and increase the level of thermal insulation inside the pore.

As a practical example, these surface-modified alumina films are then used as templates for electrodeposition of an established thermoelectric material, Bi_2Te_3. This approach to pore narrowing is a useful middle ground between the precise control of pore diameter via ALD methods and the cost-effectiveness and industrial scalability of traditional sol−gel dip methods and can serve as a starting point for applications that require alteration of the pore surface. This type of method is the opposite of the approach of wet etching, in which the pore walls are dissolved down rather than built up. Our approach offers two distinct advantages over wet etching, including compatibility with thick films of porous alumina and efficient processing for methods that involve a modified surface. Thick nanowire templates have advantages in device incorporation, and if the extent of sol−gel reaction inside the pores is limited, the coating thickness should be even throughout the full length of the pore. Additionally, we can use the choice of coating material to other desirable ends, such as thermally insulating the nanowires from the porous aluminum oxide template. In applications in which a new surface is desirable, the coating method of pore narrowing can combine size specificity and surface changes in one efficient step. Both layers in our work, silane and polymer, do impose limits based upon their thermal stability and are not well-suited for applications that require high-temperature processing.[34] However, there are many nanowire applications of porous aluminum oxide, such as electrodeposition, that use temperatures compatible with the different coatings, including our test system of thermoelectric Bi_2Te_3.

EXPERIMENTAL SECTION

All reagents were used as purchased unless otherwise noted. Sheets of aluminum foil (0.13 mm thick, 99.9995% pure) were purchased from Alfa Aesar. Aluminum films were mechanically polished to a mirror finish in a two-stage treatment, first with Metadi II diamond polish (1 μm particle size) and then with Allied colloidal silica (0.05 μm particle size). Polished Al films underwent a double anodization procedure as described by Masuda[35] to form porous alumina with a normative pore size of 40 nm. The Al film was initially anodized at 40 V and room temperature for 6 h in an aqueous solution of 0.2 M oxalic acid (solid oxalic acid from Alfa Aesar, 99.5% pure). The initial porous alumina film was treated with a heated acidic solution (2 g of CrO_3, 95 mL of H_3PO_4, and 5 mL of H_2SO_4) for 15 min to remove the existing porous structure. After the alumina had been dissolved away, the remaining Al film was anodized again at 40 V in a 0.2 M oxalic acid solution at 0 °C for 36 h. Oxalic acid was used for alumina fabrication primarily because the individual expertise and laboratory infrastructure supported the fastest turnaround on high-quality films grown in this acid. The typical thickness of porous alumina films created in this manner is 60 μm. At this stage, excess aluminum was stripped from the porous aluminum film by immersion in an aqueous saturated $HgCl_2$ solution.

Some porous alumina films were sent to Thin Film Technology Corp. where a Ti/Pt film was sputter-deposited onto the nonbarrier layer side of the porous alumina utilizing a proprietary methodology. When porous alumina films received the treatment, this step was inserted between the second 40 V anodization and the $HgCl_2$

treatment. The Pt/Ti film was coated with clear fingernail polish before the $HgCl_2$ treatment to prevent interaction of the metallic thin film with the mercury. After the mercuric chloride step, the barrier layer of the Pt/Ti-backed porous alumina was then removed by immersion in a rapidly stirred 10% H_3PO_4 aqueous solution for 70 min.

Porous alumina films ready for silanization were pretreated by being immersed in a soaking solution for at least 1 h to allow full permeation of the solution into the pores. The soaking solution was a predetermined mixture of water and methanol, ranging from 100% water to 100% methanol. Aqueous buffer solutions were made by equimolar mixing of either acetic acid/sodium acetate or sodium bicarbonate/sodium carbonate solutions.

3-Aminopropyltriethoxysilane (Aldrich, 99% pure) was dissolved in toluene (Fisher) for silanization treatments. The APTES concentration ranged from 0.01 to 10% silane (v/v). Silane solutions were used under a nitrogen atmosphere. The soaked porous alumina was immersed in the silane solution for 5−120 min and then rinsed thoroughly with methanol. Afterward, the membranes were floated upon a viscous solution of saturated KOH (Aldrich) in ethylene glycol to clear any pore opening blocked by silane buildup.

For the addition of poly(methyl methacrylate), 1 g of PMMA (MW ∼ 350K g/mol, Aldrich) was added to 100 mL of tetrahydrofuran (Fisher). The silanized porous alumina film was immersed into the solution and then stirred and heated under reflux conditions at 80 °C for 24 h. Afterward, the porous alumina film was floated on a concentrated base as in the silane preparation, and then the modified film was soaked in acetone for 10 min to remove PMMA that is noncovalently associated with the surface.

Electrodeposition of nanowires was achieved by application of the porous alumina-masked Pt/Ti films described above. With the pores open, the metal−alumina electrode was affixed to a copper disk electrode with colloidal Ag paint (Ted Pella). The copper electrode itself was coated with either fingernail polish or paraffin, depending on the aqueous or organic nature of the electrodeposition conditions, respectively. In all electrodepositions, a three-electrode setup was used: the Pt-backed alumina template as the working electrode, a piece of Pt gauze as a counter electrode, and a homemade Ag/AgCl (3 M NaCl) reference electrode with a measured potential of 0.209 V versus the standard hydrogen electrode. For depositions in which DMSO was the solvent, a Pt wire pseudoreference electrode was used in place of the Ag/AgCl electrode. Porous alumina electrodes were soaked in the electrodeposition solution with vigorous stirring for at least 1 h to ensure the penetration of the solution into the pores. Electrodepositions were conducted potentiostatically on homemade potentiostats.

The electrodeposition of Bi_2Te_3 nanowires is described well in the literature.[20,28,36−39] A mass of 0.392 g of Bi metal (Mallinckrodt) and 0.319 g of Te metal (Aldrich, 99.8% pure) were dissolved in 15.75 mL of concentrated HNO_3. This solution was stirred until the metals had completely reacted with the nitric acid to form Bi^{3+} and $HTeO_2^+$. The mixture was subsequently diluted with water to 250 mL. The three-electrode setup was used with the Ag/AgCl reference electrode in a 1 M KNO_3 solution connected to the deposition solution and the other two electrodes through a salt bridge (the salt bridge was made by heating a slurry of 2.5275 g of KNO_3, 0.75 g of agar, and 25 mL of H_2O until a gel-like consistency was obtained and then carefully poured into a curved glass tube to cool). Both solutions were cooled by a circulating ice−water bath prior to and during the experiment; this minimized acid-derived pore widening in the alumina during the soaking phase and maintained a sufficient rate of reduction during the electrodeposition process. An applied voltage of −0.019 V versus the Ag/AgCl electrode was applied for a typical time of 3−4 h, until nanowire overgrowth was visible on the template surface.

Scanning electron microscopy (SEM) was used for visualization of nanostructured features of samples made in this work. A Hitachi S-5000 scanning electron microscope operating at 10 keV, courtesy of the Electron Microscopy Lab of the University of California at Berkeley, was utilized. Secondary electron and backscatter electron detectors were used in this work. SEM samples were sputter-coated with a thin Pt layer using a Tousimis Sputter Coater linked to a Bio-Rad E5400 Controller. X-ray diffraction data were obtained with a D5000 Siemens X-ray diffractometer utilizing 1.54 Å Cu Kα radiation.

RESULTS AND DISCUSSION

There are many variables that can be altered for sol−gel techniques, including dip time, reagent concentration, and different drying and annealing procedures. Although this is a nontraditional dip coating method, these variables can still affect the resulting coats and need to be studied to establish a procedure for obtaining coated pores with precise diameters. Careful control of the silanization process will be shown to allow for many different controls of pore diameter, roughness, and coating quality.

The H_2O:$HOCH_3$ ratio in the presoaking solution is an important factor in determining the coating thickness on the pore walls because the ratio will determine how much water is available for silane cross-linking reactions. Figure 2 shows

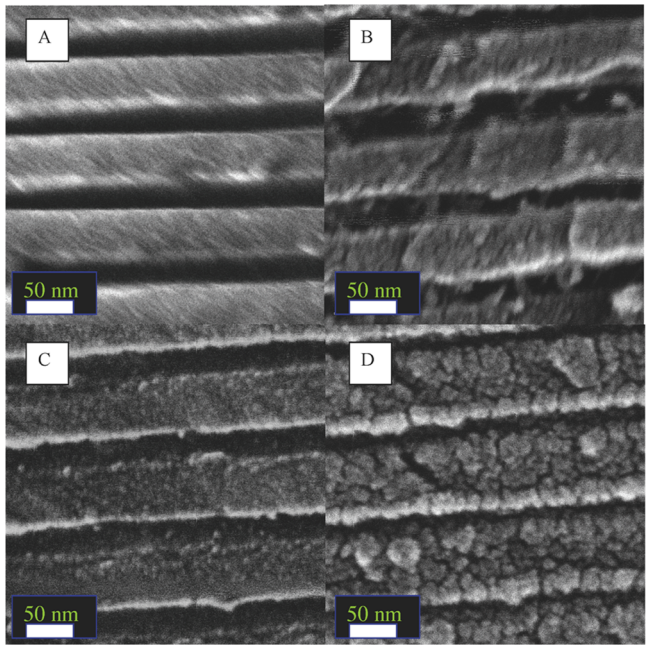

Figure 2. SEM images of porous alumina treated with APTES and a presoak treatment: (A) 8, (B) 50, (C) 75, and (D) 100% water. Horizontal gray areas represent the alumina and coating, while horizontal black columns are the pores.

porous alumina that has been treated with APTES under varying initial soak conditions. In these experiments, the samples were exposed to the APTES solution for 60 min at room temperature. There is a clear trend of decreasing pore size with increasing water content in the soaking solution. As water content decreases, the APTES has less available reagent for cross-linking of APTES molecules, resulting in less filling of pores. The methanol cannot facilitate cross-linking because it is unable to bridge between silicon centers.

The soaking solution allows for a decrease in pore width in our templates of up to 18 nm, illustrated graphically in Figure 3 as a function of average pore diameter. Although there is some overlap of error bars, a clear trend toward smaller pore diameters with an increasing level of water is exhibited. The presence of empty pore space with 100% water soaks can be explained by a combination of diffusion of water out of the

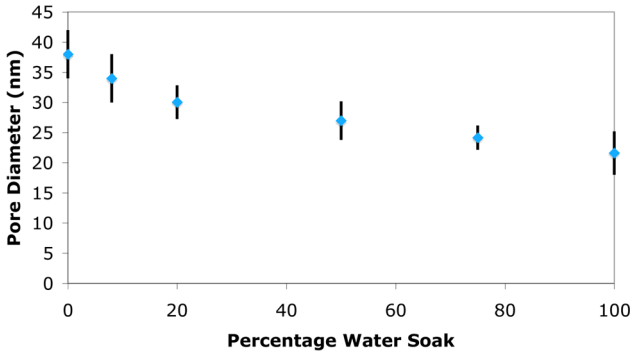

Figure 3. Average porous alumina pore diameter and standard deviation after APTES treatment as a function of the water content of the presoaking solution.

pores and chemical equilibrium limiting the maximal extent of silane cross-linking.

Results from changes in conditions other than presoak water content are summarized in Table 1. There were no statistical differences of modified pore width with the starting concentration of APTES under the conditions studied. This is likely because water is the limiting reagent in APTES cross-linking on the pore wall. The lack of APTES concentration dependence is also consistent with the lack of correlation between coating thickness and longer APTES treatment times; at times of >15 min, there is no water for further reaction. Below 15 min, measured pore diameters were inconsistent across different areas of the sample. This may be due to a mass-transfer issue, where a minimal time is required for APTES to diffuse through the nanoporous structure.

Table 1. Average Pore Diameters at Different APTES Concentrations and Reaction Times

percent H_2O soak	APTES % (v/v)	immersion time (min)	average pore diameter (nm)
100	2	60	22 (4)
100	1	60	22 (5)
100	0.25	60	23 (4)
100	10	60	22 (4)
100	2	15	22 (5)
100	2	30	23 (4)
100	2	110	22 (4)

Beyond 15 min, the distance from the alumina surface did not exhibit a statistically significant effect upon the extent of pore narrowing, except in areas very near (<5 μm) the surface with open pores. The silane layer can agglomerate at the pore openings, nearly closing or closing pores. This phenomenon prevents further use of the modified porous structure, so a further treatment is necessary to reopen those pores. Therefore, after APTES treatment, pores were floated on a concentrated KOH/ethylene glycol solution for 2−3 min to ensure the pores were open afterward.

Methanol was the primary cosolvent used in the presoak solution studies. Dimethyl sulfoxide and acetone solvents were also studied as cosolvents with water in the soaking solution and exhibited no effect on the extent of silanization. This may suggest a high adaptability of this method toward other sol−gel reactions with more specific solvent requirements.

The range of pore widths can be expanded with multiple treatments of APTES. The porous alumina template, once coated, still has available oxo sites on the pore walls from the APTES that can undergo further cross-linking. Figure 4 shows a progression of silanization, with panel A representing a single treatment (100% H_2O presoak) and panel B representing a double treatment (both 100% H_2O pretreatment conditions). Both coating treatments involved dipping the template into the silane solution for 60 min. This second silanization treatment narrows the average pore diameter by a further 10 nm, from 22 to 12 nm.

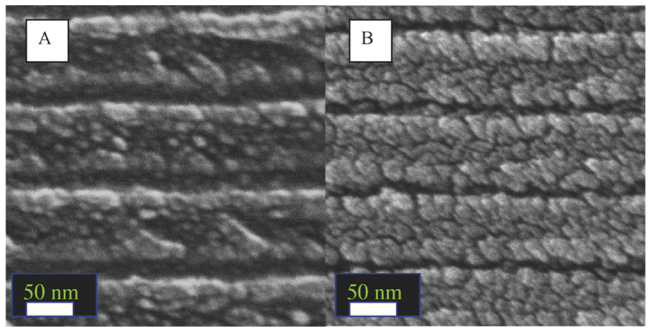

Figure 4. SEM images of porous alumina treated with (A) one water soak/APTES treatment and (B) two sequential soak/APTES treatments.

The acidity or basicity of the soak solution plays an important role in the process of coating the pore walls. Figure 5 shows the pore diameters of coated porous alumina when the soak solution is buffered with a 1:1 HOAc/NaOAc (pK_a = 4.74) or $NaHCO_3/Na_2CO_3$ (pK_a = 10.3) solution at a total buffer concentration of 0.10 M. The pores soaked in the acetate buffer, shown in Figure 5A, have pore diameters of 30 (2) nm, larger than the pores prepared with unbuffered water [22 (4) nm]. The pores soaked in carbonate buffer have even smaller

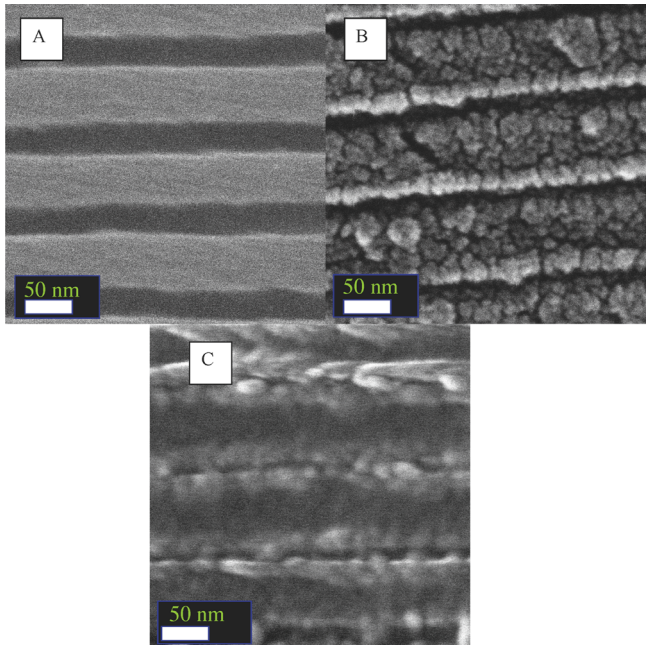

Figure 5. SEM images of porous alumina treated with APTES after being soaked in (A) a 0.05 M HOAc/0.05 M NaOAc aqueous buffer solution, (B) unbuffered water, and (C) a 0.05 M $NaHCO_3$/0.05 M Na_2CO_3 aqueous buffer solution.

pore diameters, ranging from 10 nm to possibly closed in some parts of the pores (Figure 5C).

These different pore diameters seen in Figure 5 can be explained in light of the differing effects of acid and base catalysis upon silane sol–gel reactions.[40] Acid catalysis can promote the formation of dense, highly cross-linked silane films, whereas the base-catalyzed reactions can produce lower-density silica solids. This is based on the nature of the gel particles; the thin, spindly gel particles formed under acidic conditions can condense and be deformed in ways that allow for efficient packing of silica, while the larger, base-generated gel particles have less space-efficient options for their final condensation. In our work, this results in thinner, denser coats of silane under acidic conditions and larger, less dense coatings under basic conditions.

Additional evidence of density differences comes from data obtained from annealing coated porous alumina for 2 h at 150 °C after silanization. Figure 6 demonstrates the effect of

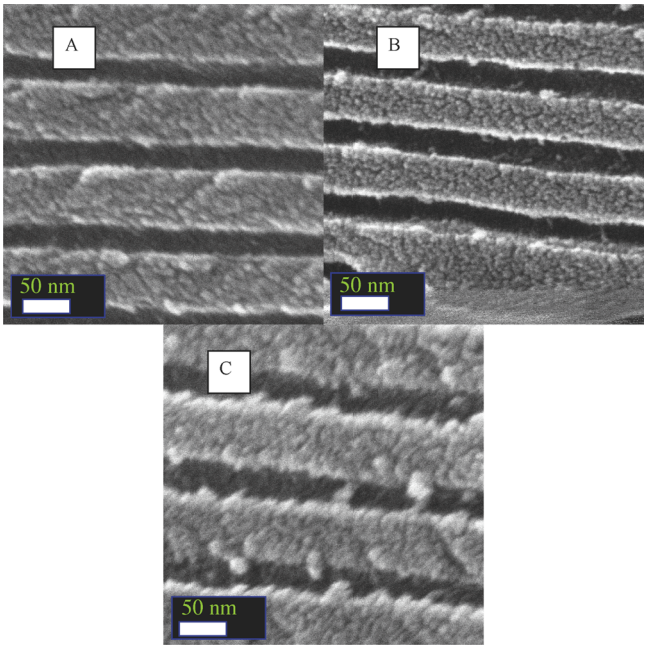

Figure 6. SEM images of samples A–C from Figure 5 after annealing in air at 150 °C for 1.5 h.

annealing porous alumina films that have been coated with APTES. Postannealing of traditional sol–gel-derived silica[41] drives off solvent and promotes further cross-linking, increasing the overall density of the silica by reducing the volume of the solid. The size of postannealed pore diameters in an unbuffered solution is statistically similar to the coating derived from the acetate buffer soak seen in Figure 5A. Figure 6C shows the carbonate buffer-presoaked sample from Figure 5C after annealing.

All samples coated with a 100% water soak solution adjust to 29 (4) nm diameter pores after annealing, regardless of the buffer conditions of the solution. There is also a visible smoothing of most of the surfaces after annealing, likely because of the opportunity for surface energy minimization. The carbonate buffer-soaked alumina does exhibit some extra intermittent debris along the pore walls; this is presumably a mechanical consequence of the extreme density gains upon annealing.

We also utilized the surface amines of the APTES coating for further pore modification. The attachment of PMMA is enacted through transformation of the ancillary ester into an amide via the amines on the APTES-coated pore walls. The reaction is shown in eq 1. In this case, R_1 is the polymer backbone and R_2 is the propyl group of the silane immobilized on the pore wall.

$$R_1\text{-}C(O)O\text{-}Et + H_2N\text{-}R_2 \rightarrow R_1\text{-}C(O)NHR_2 + HOEt \quad (1)$$

This is a thermodynamically favored transformation due to the larger extent of delocalization of the nitrogen lone pair into the carbonyl system, as compared to that of the oxygen lone pair of the ester. This transformation has kinetic limitations because of the difficulty in coordinating the transfer of a proton between the oxygens and nitrogens involved. This kinetic barrier can be overcome with heat and time in the form of overnight reflux. The end result is a long-chain polymer covalently attached to the pore wall with a chemically resilient amide bond.

Micrographs for PMMA-treated templates are shown in Figure 7. The images show the changes in pore wall

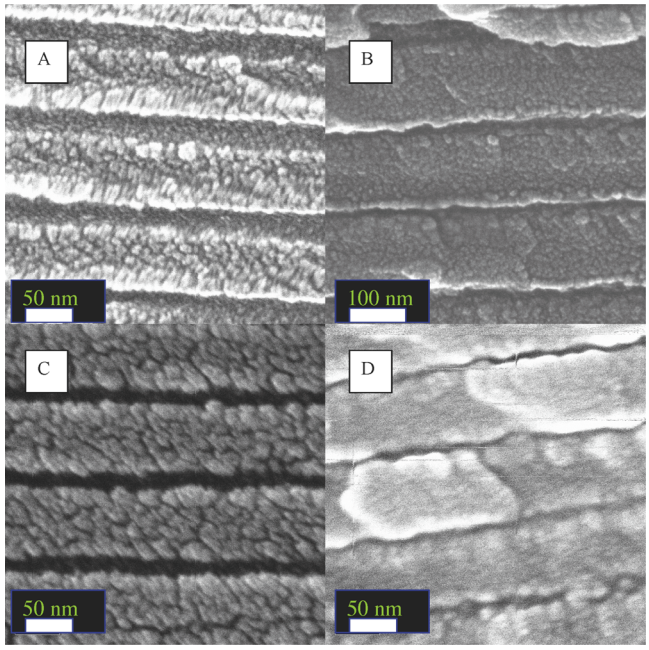

Figure 7. SEM images of silanized pores before and after PMMA treatment: (A) porous alumina silanized after a 100% H_2O soak, (B) subsequent PMMA treatment of sample A, (C) porous alumina silanized twice (100% H_2O soaks), and (D) subsequent PMMA treatment of sample C.

morphology and the change in pore size, supporting the claim that PMMA attaches to the APTES-derived film. The inclusion of a proton-transfer catalyst (hydroxypyridone)[42] had no apparent effect on the films formed, and variation of temperature from 80 to 110 °C also had no observed effect. The pores are narrower after PMMA treatment, decreasing to from 22 (4) to 12 (5) nm in templates that were treated with APTES under 100% water presoak conditions. The alumina that underwent two silane treatements (both 100% water presoak) went from 12 (4) to <8 nm, beyond the reasonable resolution of our SEM detector.

Dissolution of porous alumina templates after the creation of polymer nanotubes has been used to further examine the

nanostructure and morphology of the nanotubes. Attempts to remove the PMMA nanotubes from the porous alumina template with either strong acid or base were unsuccessful. The resultant debris shows no signs of tubule-like structures. This provides support to the covalent linkage of PMMA to the pore wall rather than van der Waals association seen in other polymer nanotubes.[43−45] We hypothesize that, if the nanotube was being held together with van der Waals forces, these organizing forces would continue to exist after the removal of the template. There would not likely be fully intact 60 μm long nanotubes (due to the small diameter and thickness of the nanotubes), but we would expect small chunks with intact tubular structure. While there would be some van der Waals associations in a covalently bound monolayer, the van der Waals forces are not the structural forces that hold the nanotube together. In this case, by destroying the surface to which the PMMA is attached, we in turn destroy the nanotubular organization of the macromolecules; the non-optimized van der Waals forces that are present are simply not able to hold even small parts of the nanostructure together after the alumina scaffold is removed.

The APTES-modified porous alumina films were used as templates for nanowires grown via electrodeposition. Porous alumina templates synthesized in oxalic acid with an initial pore diameter of 40 nm were used in the coating procedures. The silanization process was performed after anodized templates were sent to Thin Film Technologies, where a thin Pt/Ti film was affixed to the porous alumina to function as an electrode surface within the pores. Because of the demonstrative purpose of these experiments, the nanowire procedures used were from literature and generally unaltered; the optimization of electrodepostion conditions for the new pore sizes could produce templates with greater numbers of nanowires with an even growth front.

The conditions of Bi_2Te_3 electrodeposition are acidic, with approximately 0.1 M HNO_3 in solution. Images of the Bi_2Te_3 nanowires are shown in Figure 8. The planar view shows a high percentage of pore filling, as well as small wires. The cross-sectional views show nanowires with the desired structural roughness and appropriately reduced diameters. Given the nature of electrosynthesis, there is little concern about the electrical continuity along the rough-looking wires; any break in conductivity would stop the wire growth. The average diameter for the wires grown in a 100% water presoak-silanized template is 22 (6) nm. This standard deviation is larger than that of the empty templates but may be attributable to the lower resolution of backscatter imaging as opposed to secondary electron imaging. The powder X-ray diffraction pattern of the nanowires inside the modified template is shown in Figure 9. Preferential ordering is in the 110 direction, consistent with Bi_2Te_3 nanowires grown in untreated templates.[46]

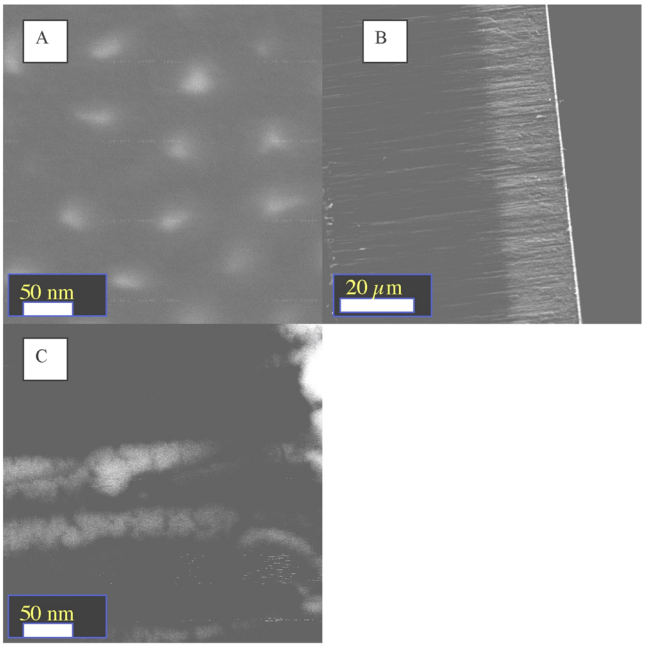

Figure 8. SEM images of Bi_2Te_3 nanowires with backscatter imaging. (A) Planar view after removal of the Pt backing electrode. (B) Cross section of wires. (C) Close-up cross section of wires.

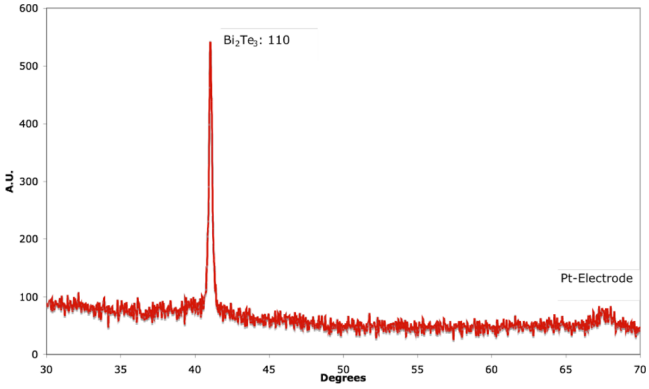

Figure 9. X-ray diffraction pattern of Bi_2Te_3 nanowires grown in a silanized porous alumina template.

CONCLUSIONS

We have detailed a process for coating porous alumina with nanometer-scale precision. The control of water concentration and pH of the pretreatment soaking solution has a strong influence on the coating thickness. The pH-related changes in coating thickness are normalized with a post-treatment annealing procedure, suggesting that coating density is the cause of variation. APTES concentration and cosolvent choices did not affect the coating within the parameters studied, and the sol−gel reaction time has no significant effect after the appropriate time for reagent diffusion has passed. We have demonstrated various solution-based variables for control of APTES thickness and developed a new method for attachment of organic molecules to the APTES surface. Additionally, nanowires of Bi_2Te_3 have been synthesized in APTES-modified templates. These nanowires have their diameter controlled by the dimensions of these modified templates. With the ability to control pore diameter, we provide a new tool for material scientists wishing to study the effect of nanometer scaling on a multitude of physical phenomenon such as thermoelectric, magnetoresistive, and photovoltaic materials.

AUTHOR INFORMATION

Corresponding Author

*E-mail: kellydn@iun.edu.

Present Addresses

†D.N.K.: Department of Chemistry, Physics, and Astronomy, Indiana University Northwest, 3400 Broadway, Gary, IN 46408-1197.

‡R.H.W.: Baker Laboratory, Department of Chemistry, Cornell University, Ithaca, NY 14853-1301.

Notes

The authors declare no competing financial interest.

■ ACKNOWLEDGMENTS

We thank Dr. G. Min and the Berkeley Electron Microscope Lab for SEM resources and assistance and Dr. S. Pedersen for conversations concerning amide formation chemistry.

■ ABBREVIATIONS

APTES, 3-aminopropyltriethoxysilane
PMMA, poly(methyl methacrylate)
SEM, scanning electron microscopy
XRD, X-ray diffraction

■ REFERENCES

(1) Edwards, J. D.; Keller, T. The Structure of Anodic Oxide Coatings. *Trans. Am. Inst. Min., Metall. Pet. Eng.* **1944**, *156*, 288−299.
(2) Keller, F.; Hunter, M. S.; Robinson, D. L. Structural Features of the Oxide Coatings on Aluminum. *J. Electrochem. Soc.* **1953**, *100*, 411−419.
(3) Lee, W.; Park, S. J. Porous Anodic Aluminum Oxide: Anodization and Templated Synthesis of Functional Nanostructures. *Chem. Rev.* **2014**, *114*, 7487−7556.
(4) Lee, W.; Ji, R.; Gösele, U.; Nielsch, K. Fast Fabrication of Long-Range Ordered Porous Alumina Membranes by Hard Anodization. *Nat. Mater.* **2006**, *5*, 741−747.
(5) Lee, W.; Schwirn, K.; Steinhart, M.; Pippel, E.; Scholz, R.; Gösele, U. Structural Engineering of Nanoporous Anodic Aluminum Oxide by Pulse Anodization of Aluminum. *Nat. Nanotechnol.* **2008**, *3*, 234.
(6) Milka, P.; Krest, I.; Keusgen, M. Immobilization of alliinase on porous aluminum oxide. *Biotechnol. Bioeng.* **2000**, *69*, 344−348.
(7) Itoh, T.; Ishii, R.; Hanaoka, T.; Hasegawa, Y.; Mizuguchi, J.; Shiomi, T.; Shimomura, T.; Yamaguchi, A.; Kaneda, H.; Teramae, N.; Mizukami, F. Encapsulation of Catalase into Nanochannels of an Inorganic Composite Membrane. *J. Mol. Catal. B: Enzym.* **2009**, *57*, 183−187.
(8) Yang, K.; Kim, H.; Ahn, J.; Kim, D. Microfluidic Chip with Porous Anodic Alumina Integrated with PDMS/Glass Substrate for Immuno-Diagnosis. *Curr. Appl. Phys.* **2009**, *9*, e60−e65.
(9) Hernandez, A.; Calvo, J.; Pradanos, P.; Palacio, L.; Rodriguez, M.; de Saja, J. Surface Structure of Microporous Membranes by Computerized SEM Image Analysis Applied to Anopore Filters. *J. Membr. Sci.* **1997**, *137*, 89−97.
(10) Leung, S.-F.; Yu, M.; Lin, Q.; Kwon, K.; Ching, K.-L.; Gu, L.; Yu, K.; Fan, Z. Efficient Photon Capturing with Ordered Three-Dimensional Nanowell Arrays. *Nano Lett.* **2012**, *12*, 3682−3689.
(11) Hirai, S.; Aizawa, S.; Shimakage, K.; Wada, K. Alkaline Corrosion Resistance of Aluminum Anodic Oxide Film Coatedwith Zirconium Oxide by a Sol-Gel Process. *Nippon Kinzoku Gakkaishi* **1995**, *59*, 547−553.
(12) Lakshmi, B.; Patrissi, C.; Martin, C. Sol−Gel Template Synthesis of Semiconductor Oxide Micro- and Nanostructures. *Chem. Mater.* **1997**, *9*, 2544−2550.
(13) Chen, R.; Xu, D.; Guo, G.; Gui, L. Silver Selenide Nanowires by Electrodeposition. *J. Electrochem. Soc.* **2003**, *150*, G183−G186.
(14) Huang, X.; Li, G.; Dou, X.; Li, L. Magnetic Properties of Single Crystalline Co Nanowire Arrays with Different Diameters and Orientations. *J. Appl. Phys.* **2009**, *105*, 084306.
(15) Dellis, S.; Christoulaki, A.; Spiliopoulos, N.; Anastassopoulos, D. L.; Vradis, A. A. Electrochemical Synthesis of Large Diameter Monocrystalline Nickel Nanowires in Porous Alumina Membranes. *J. Appl. Phys.* **2013**, *114*, 164308.
(16) Masuda, H.; Takenaka, K.; Ishii, T.; Nishio, K. Long-Range-Ordered Anodic Porous Alumina with Less-than-30 nm Hole Intervals. *Jpn. J. Appl. Phys.* **2006**, *45*, L1165−L1167.
(17) Nishinaga, O.; Kikuchi, T.; Natsui, S.; Suzuki, R. O. Rapid Fabrication of Self-Ordered Porous Alumina with 10-/Sub-10-nm-Scale Nanostructures by Selenic Acid Anodizing. *Sci. Rep.* **2013**, *3*, 2748.
(18) Manzano, C. V.; Martin, J.; Martin-Gonzalez, M. S. Ultra-Narrow 12 nm Pore Diameter Self-Ordered Anodic Alumina Templates. *Microporous Mesoporous Mater.* **2014**, *184*, 177−183.
(19) Wang, C. E.; Tanaka, S.; Shimizu, T.; Shingubara, S. Fabrication of Vertical Cu_2ZnSnS_4 Nanowire Arrays by Two-Step Electroplating Method into Anodic Aluminum Oxide Template. *Journal of Materials Science & Nanotechnology* **2014**, *1*, S103.
(20) Trahey, L.; Becker, C.; Stacy, A. Electrodeposited Bismuth Telluride Nanowire Arrays with Uniform Growth Fronts. *Nano Lett.* **2007**, *7*, 2535−2539.
(21) Zhou, Y.; Shen, C.; Li, H. Synthesis of High-Ordered $LiCoO_2$ Nanowire Arrays by AAO Template. *Solid State Ionics* **2002**, *146*, 81−86.
(22) Martin, J.; Manzano, C. V.; Caballero-Calero, O.; Martin-Gonzalez, M. High-Aspect-Ratio and Highly Ordered 15-nm Porous Alumina Templates. *ACS Appl. Mater. Interfaces* **2013**, *5*, 72−79.
(23) Keyani, J.; Stacy, A. Assembly and Measurement of a Hybrid Nanowire-Bulk Thermoelectric Device. *Appl. Phys. Lett.* **2006**, *89*, 233106.
(24) Dresselhaus, M.; Dresselhaus, G.; Sun, X.; Zhang, Z.; Cronin, S.; Koga, T. Low Dimensional Thermoelectric Materials. *Phys. Solid State* **1999**, *41*, 679−682.
(25) Hicks, L.; Dresselhaus, M. Thermoelectric Figure of Merit of a One-Dimensional Conductor. *Phys. Rev. B* **1993**, *47*, 16631−16634.
(26) Lin, S.; Sun, X.; Dresselhaus, M. Theoretical Investigation of Thermoelectric Transport Properties of Cylindrical Bi Nanowires. *Phys. Rev. B* **2000**, *62*, 4610−4623.
(27) Wei, C.; Yang, L.; Chou, M. Quantum Confinement and Electronic Properties of Silicon Nanowires. *Phys. Rev. Lett.* **2004**, *92*, 236805.
(28) Hochbaum, A.; Chen, R.; Delgado, R.; Liang, W.; Garnett, E.; Najaran, M.; Majumdar, A.; Yang, P. Enhanced Thermoelectric Performance of Rough Silicon Nanowires. *Nature* **2008**, *451*, 163.
(29) Elam, J.; Liera, J.; Pellin, M.; Stair, P. Spatially Controlled Atomic Layer Deposition in Porous Materials. *Appl. Phys. Lett.* **2007**, *91*, 243105/1−243105/3.
(30) Xiong, G.; Elam, J.; Feng, H.; Han, C.; Wang, H.; Iton, L.; Curtiss, L.; Pellinn, M.; Kung, M.; Stair, P. Effect of Atomic Layer Deposition Coatings on the Surface Structure of Anodic Aluminum Oxide Membranes. *J. Phys. Chem. B* **2005**, *109*, 14059−14063.
(31) Li, A. P.; Müller, F.; Birner, A.; Nielsch, K.; Gösele, U. Hexagonal Pore Arrays with a 50−420 nm Interpore Distance Formed by Self-Organization in Anodic Alumina. *J. Appl. Phys.* **1998**, *84*, 6023.
(32) Zhang, J.; Kielbasa, J. E.; Carroll, D. L. Controllable Fabrication of Porous Alumina Templates for Nanostructures Synthesis. *Mater. Chem. Phys.* **2010**, *122*, 295−300.
(33) Ersching, K.; Dorico, E.; da Silva, R. C.; Zoldan, V. C.; Isoppo, E. A.; Viegas, A. D. C.; Pasa, A. A. Surface and Interface Characterization of Nanoporous Alumina Templates Produced in Oxalic Acid and Submitted to Etching Procedures. *Mater. Chem. Phys.* **2012**, *137*, 140−146.
(34) Jie, J.; Wang, G.; Wang, O.; Chen, Y.; Han, X.; Wang, X.; Hou, J. G. Synthesis and Characterization of Aligned ZnO Nanorods on Porous Aluminum Oxide Templates. *J. Phys. Chem. B* **2004**, *108*, 11976−11980.
(35) Masuda, H.; Satoh, M. Fabrication of Gold Nanodot Array using Anodic Porous Alumina as an Evaporation Mask. *Jpn. J. Appl. Phys.* **1996**, *35*, 126−129.
(36) Prieto, A.; Sander, M.; Martin-Gonzalez, M.; Gronsky, R.; Sands, T.; Stacy, A. Electrodeposition of Ordered Bi_2Te_3 Nanowire Arrays. *J. Am. Chem. Soc.* **2001**, *123*, 7160−7161.
(37) Martin-Gonzalez, M.; Prieto, A.; Gronsky, R.; Sands, T.; Stacy, A. Insights into the Electrodeposition of Bi_2Te_3. *J. Electrochem. Soc.* **2002**, *149*, 335−339.

(38) Li, S.; Liang, Y.; Qin, J.; Toprak, M.; Muhammed, M. Template Electrodeposition of Ordered Bismuth Telluride Nanowire Arrays. *J. Nanosci. Nanotechnol.* **2009**, *9*, 1543−1547.
(39) Mavrokefalos, A.; Moore, A. L.; Pettes, M. T.; Shi, L.; Wang, W.; Li, X. Thermoelectric and Structural Characterizations of Individual Electrodeposited Bismuth Telluride Nanowires. *J. Appl. Phys.* **2009**, *105*, 104318.
(40) Iler, R. K. *The Chemistry of Silica: Solubility, Polymerization, Colloid and Surface Properties, and Biochemistry*, 1st ed.; Wiley: New York, 1979.
(41) Brinker, C.; Scherer, G. *Sol-Gel Science*, 1st ed.; Academic Press: San Diego, 1990.
(42) Fischer, C.; Steininger, H.; Stephenson, D.; Zipse, H. Catalysis of Aminolysis of p-Nitrophenyl Acetate by 2-Pyridones. *J. Phys. Org. Chem.* **2005**, *18*, 901−907.
(43) Cepak, V.; Martin, C. Preparation of Polymeric Micro-and Nanostructures Using a Template-Based Deposition Method. *Chem. Mater.* **1999**, *11*, 1363−1367.
(44) Shin, K.; Obukhov, S.; Chen, J.; Huh, J.; Hwang, Y.; Mok, S.; Dobriyal, P.; Thiyagarajan, P.; Russell, T. Enhanced Mobility of Confined Polymers. *Nat. Mater.* **2007**, *6*, 961.
(45) Song, G.; She, X.; Fu, Z.; Li, J. Preparation of Good Mechanical Property Polystyrene Nanotubes with Array Structure in Anodic Aluminum Oxide Template Using Simple Physical Techniques. *J. Mater. Res.* **2004**, *19*, 3324−3328.
(46) Sander, M.; Gronsky, R.; Sands, T.; Stacy, A. Structure of Bismuth Telluride Nanowire Arrays Fabricated by Electrodeposition into Porous Anodic Alumina Templates. *Chem. Mater.* **2003**, *15*, 335−339.